3D Geomechanical Analysis of Multiple Caverns in Bedded Salt

by

Michael Bruno, Luis Dorfmann, Gang Han, Khang Lao, and Jean Young

Terralog Technologies USA, Inc.
Arcadia, California 91006 USA
(626) 305-8460; www.terralog.com

SMRI Fall 2005 Meeting
October 1-5, 2005
Nancy, France

Solution Mining Research Institute, Fall 2005 Technical Meeting
Nancy, France, October 1-5, 2005

3D Geomechanical Analysis of Multiple Caverns in Bedded Salt

Michael Bruno, Luis Dorfmann, Gang Han, Khang Lao, and Jean Young
Terralog Technologies USA, Inc.
332 E. Foothill Blvd, Arcadia CA, 91006 USA

ABSTRACT

This paper summarizes results from a recently concluded research project sponsored by the Gas Research Institute, the Petroleum Research Technology Council, and the US Department of Energy. The primary objective of this work has been to improve the state-of-the-art for designing and operating single and multiple caverns in thin bedded salt formations. The effort has included a geologic and geomechanical review of the Permian, Michigan, and Appalachian basins, followed by geomechanical modeling for single and multiple caverns in layered media.

A modified creep viscoplastic model has been developed and implemented in Flac3D to simulate bedded salt material behavior. Both cyclic pressure operations and direct pressure drawdown are simulated. Cavern design parameters are varied to evaluate how they influence propagation of damage and the deformation of cavern. These are the cavern pressure, operating conditions, cavern size expressed in terms of height/diameter (H/D) ratio, overburden stiffness and roof thickness. The baseline results for single cavern simulations illustrate a shear stress distribution primarily around the cavern top and bottom corners, salt damage mainly around the cavern sidewall and slippage in the top interface between the salt formation and the anhydrite layer. During cyclic pressure operations, the shear-stress zones propagate into a wider region, which is responsible for an increase in the amount of slippage in the interface. During cyclic pressure loading, the magnitude of the maximum shear stress does not increase, resulting in no additional damage (micro-cracks) in the surrounding salt.

The influence of the overburden stiffness is shown to be a critical parameter on the overall cavern response. A substantial part of the weight of the overburden material is carried by the anhydrite layer and by the cavern roof itself. For this particular case, the anhydrite reaches it tensile limit and fails. This failure implies that the cavern roof is subjected to a much higher load and therefore the amount and extension of damage increases substantially.

We further evaluate minimum safe center to center distance of multiple horizontal caverns. We find that a center to center distance of two cavern diameters is not sufficient to eliminate the mutual interaction. Increasing the center to center distance to three cavern diameters, however, generally eliminates most interaction.

1. INTRODUCTION AND BACKGROUND

Bedded salt formations are found in several areas throughout the United States and Canada, providing a useful means for storing gas near major markets (see Figure 1). The largest basins include the Permian Basin across Texas, Oklahoma, Kansas, Colorado, and New Mexico, the Gulf Coast Basin across Southern Texas, Louisiana, Mississippi, and Alabama, and the Michigan and Appalachian Basins across the states of Michigan, Ohio, Pennsylvania and New York. These areas have experienced different deposition and tectonic history, resulting in some differences in depth, lithology and typical geologic structure for the dominant bedded salt intervals.

Bedded salt formations in all areas, however, are layered and interspersed with non-salt sedimentary materials such as anhydrite, shale, dolomite, and limestone. The "salt" layers themselves also often contain significant impurities. In comparison to relatively homogeneous salt domes, therefore, cavern development and operations present additional engineering challenges related to:

- The layered, heterogeneous lithology;
- Differential deformation, creep, and bedding plane slip between individual layers;
- Somewhat larger lateral to vertical cavern dimensions.

The primary objective of this project has been to increase gas storage capabilities throughout North America by providing operators with improved geotechnical design and operating guidelines for thin-bedded salt caverns. To accomplish this objective, first, Terralog Technologies has evaluated and compiled pertinent literature on the Permian, Michigan and Appalachian Basins (Figure 1) including geology and mechanical properties for thin-bedded salt formations. All available cavern sonar surveys are collected and described from the Permian, Appalachian and Michigan Basins. In addition, we compiled regulations and guidelines governing the thin-bedded salt caverns in the United States. Another task Terralog has completed is to calibrate and implement a correct constitutive material model that matches the available strength and creep response test data in the three major salt basins. This involve modifying a creep viscoplastic material model in FLAC3D to include pseudo-elastic loading response, elastic unloading routine and failure response from salt. A baseline single cavern model has been built to incorporate this new material model. The results are analyzed and iterations are performed to match real caverns behaviors.

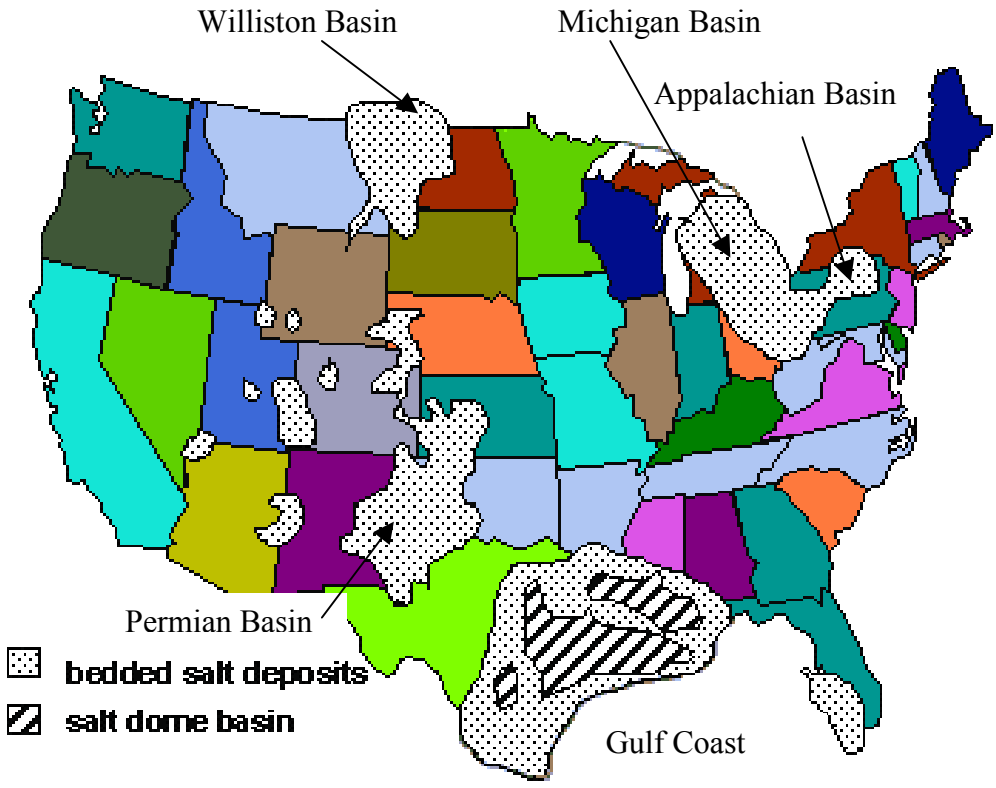

Source: National Petroleum Technology Office

Figure 1. Bedded Salt Deposits in US

2. GEOLOGIC OVERVIEW

Detailed geologic characterization is an important and necessary pre-requisite for any analytical or numerical investigations on the geomechanical processes in bedded salt formation. This process allows us to establish a realistic range of scenarios for parametric model investigations within the Permian, Michigan and Appalachian Basins:

2.1 Permian Basin Complex

Complex faulting in the mid Permian Period created platforms and arches that subdivided the Permian Basin Complex into the five separate basins: Anadarko, Palo Duro, Dalhart, Midland and Delaware Basins. At times, these basins were interconnected by shallow seaways. Marine water entered the basins from open ocean to the southwest (Johnson and Gonzales, 1978). The oldest salt, the Early Permian age Hutchison Salt Member was found in the northern Anadarko Basin, Kansas and Oklahoma border. Evaporites accumulation moved southward. By Late

Permian time, evaporite deposits had reached the Delaware and Midland Basins (Johnson and Gonzales, 1978). Basin evolution after evaporite deposition is important for salt cavern siting because the salt geometry was modified by burial dissolution (Hovorka and Nava, 2000). The Permian Basin Complex region was tectonically stable after the deposition of salts. Salt dissolution and subsequent collapse of overlying strata is common in the Permian Basin Complex. Most of the dissolution occurs within 400 m (1,300 ft) of the surface (McGookey, Gustavson and Hoadley, 1988). All the salt bearing formations within the Permian Basin Complex have been affected locally by salt dissolution.

The Midland Basin has the most salt cavern operations. Thirteen operators are actively operating approximately 100 wells within the Midland Basin. Salado is the dominant salt bearing unit where all the active caverns are found. Figure 3 is the sonar survey of a multiple caverns within the Midland Basin. The thickest Salado salt can be found in the southwestern part of the Basin in less than 600 m (2,000 ft) depth. The Queen Formation offers another potential salt unit for cavern siting where locally over 50 m (165 ft) thick salt can be found in the north. However, it is below the Salado Formation. The cost for developing the lower salt layer has to be considered when the shallow Salado salts are available.

The Salado salt is also the dominant halite unit within the Delaware Basin, however the salt is found in less than 300 m (1,000 ft) depth, too shallow for salt cavern siting. Thick salt unit may be found locally within the Castile Formation especially in the northern part of the Basin which can be used for cavern development.

The San Andres Formation is the dominant salt within the Palo Duro Basin, where over 50 m (165 ft) thick is found on the southwest side of the Basin. The top of the salt can be reached between 600-900 m (2,000-3,000 ft) from the surface. The Upper Clear Fork salt can reach 120 m (400 ft) thick locally which may offers another possible cavern siting on the eastern part of the Basin. This Basin offers potential for salt cavern development.

Within the Dalhart Basin, Blaine Formation is the dominant salt unit, found in less than 300 m (1,000 ft) depth (Johnson and Gonzales, 1987), and too shallow for cavern development. The Upper Clear Fork salt unit is not thick enough for cavern siting.

Salt caverns operations are also found in the Anadarko Basin. Two operators are actively operating over 25 wells between 425-550 m (1,400 ft to 1,800 ft) depth. The caverns are found in the main salt unit, the Lower Cimarron Salt Formation. Thirty to ninety meters (100-300 ft) thick halite can be found in the southern and eastern portion of the Basin. Other potential salt unit for cavern siting is the Hutchison Member which is found only in the northeast, where locally thick salt may be found in less than 900 m (3,000 ft) depth.

2.2 Appalachian and Michigan Basins

Throughout the Paleozoic, the Michigan Basin continued to subside faster than the Appalachian Basin and the surrounding regions (Johnson and Gonzales, 1978). A shallow sea spread over the Great Lakes region as Paleozoic Era began. The emergence of the Kankakee

Arch in the middle Silurian time greatly restricted the seawater circulation within the Michigan Basin (Michigan State University). In addition, the development of the Middle Silurian age reefs may also had restricted the marine water within the Appalachian Basin, except on the southeast side in Ohio (Johnson and Gonzales, 1978). These restrictions lead to evaporation of the sea water and the deposition of salt within the Michigan and Appalachian Basins. The Michigan Basin and the north to northwestern Appalachian Basin were tectonically stable since the beginning of the Paleozoic (Johnson and Gonzales, 1978). However, the central and southeast part of the Appalachian Basin was affected by the Appalachian Orogeny which created folded, faulted structures and tectonically thickened salt accumulations (Terralog, Dec. 30, 2001). This area is tectonically stable after the Appalachian Orogeny.

The Silurian Salina Formation is the dominant salt in both the Michigan and the Appalachian Basins. There is at least one thick salt bed over 50 m (165 ft) within 900 m (3,000 ft) from the surface in both Basins. Salt is absent in outcrop and at shallow depth in the Appalachian Basin. Abrupt thinning and termination of salt units near the Michigan Basin margins and salt core anticlines are attributed to the salt dissolution (Johnson and Gonzales, 1978). The collapses occurred within the Michigan Basin are due to cavities found within the overlying sandstones than salt dissolution (Johnson, 1986). The overlying friable sandstone formed a slurry with the groundwater; the slurry flowed downward into joints and other voids in the underlying dolomite and salt units forming cavities within the sandstone unit. When the sandstone unit can no longer span the cavity, it failed causing the overlying dolomite and glacial drift to collapse (Johnson, 1986).

In the Michigan Basin six operators operate approximately 30 caverns in the Salina salt. All wells are located within the southern rim of the Basin where the caverns are found in less than 1,200 m (4,000 ft) depth. There are at least 2 salt beds over 50 m (165 ft) thick in the Salina Formation. The Detroit River salt is too thin for cavern development.

The major salt formation in the Appalachian Basin is also the Salina Formation. Four companies are currently operating gas storage caverns in the Appalachian Basin. Three operators operate over 15 caverns in the New York State, while one operator operates one cavern with 2 wells in Ohio State. Caverns are excavated in the thick Salina salt in less than 1,050 m (3,500 ft) in the northern part of the Appalachian Basin in New York State. In Ohio State, the active cavern is located at 1,100 m (3,600 ft) depth on the western side of the Appalachian Basin.

3. SALT CAVERN OVERVIEW

All available sonar surveys from the Permian, Michigan and Appalachian Basins were acquired. The data have been summarized in Tables 1 through 4. Large caverns are found in the Midland and Michigan Basins with average capacity over 275,000 barrels. The Anadarko and Appalachian Basins have tall cylinder shape caverns with average capacity around 150,000 barrels. Figure 2 below shows a typical single cavern configuration (stack pancake shape). Figure 3 shows a sample sonar survey of a multiple vertical cavern.

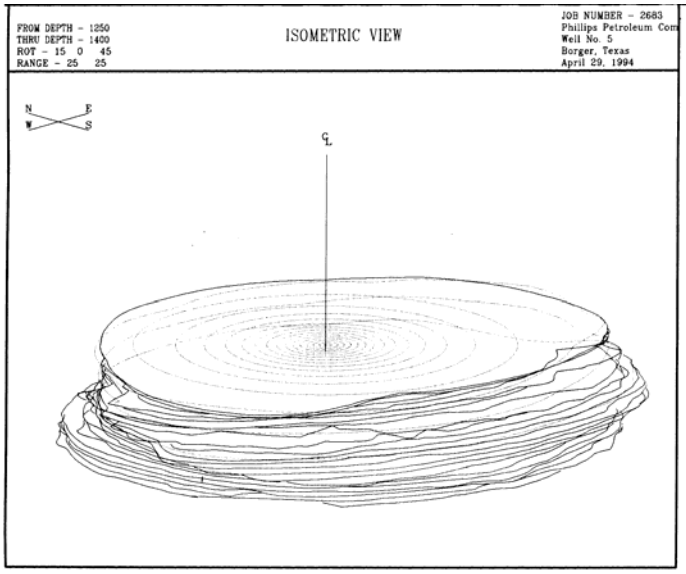

Figure 2: Typical single cavern configuration

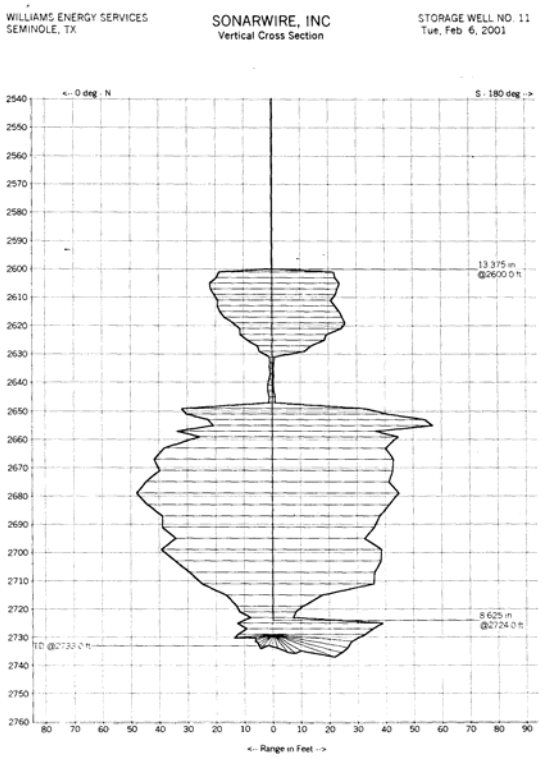

Figure 3: Sample sonar survey of a multiple vertical cavern

Table 1 Anardarko Basin Sonar Survey Summary

Company	Cavern No.	Main Roof	Bottom Depth (ft)	Ave. Height (ft)	Ave. Diameter	Cavern Volumn	Ht/W Ratio	Shape
Phillips Petroleum Co.	3	1438	1482	44	230	209,056	0.1913	cylinder
Phillips Petroleum Co.	4	1472	1528	56	266	455,591	0.2105	cylinder
Phillips Petroleum Co.	5	1331	1376	45	209	266,973	0.2153	cylinder
Phillips Petroleum Co.	6	1426	1446	20	295	243,337	0.0678	cylinder
Phillips Petroleum Co.	7	1415	1483	68	225	436,130	0.3022	cylinder
Phillips Petroleum Co.	8	1450	1474	24	270	244,609	0.0889	cylinder
Phillips Petroleum Co.	9	1447	1467	20	241	167,785	0.0830	cylinder
Phillips Petroleum Co.	10	1450	1500	50	259	457,566	0.1931	cylinder
Phillips Petroleum Co.	11	1472	1500	28	320	400,859	0.0875	upside down cone
	12a	1456	1501	45	72	32,615	0.6250	cylinder
	12b	1501	1536	35	205	205,641	0.1707	cylinder
Phillips Petroleum Co.	12					238,255		
Phillips Petroleum Co.	13	1490	1540	50	200	279,617	0.2500	
Phillips Petroleum Co.	14	1475	1525	50	180	226,490	0.2778	cylinder
Phillips Petroleum Co.	21	1426	1536	110	94	135,888	1.1702	stack pancakes
Phillips Petroleum Co.	22	1460	1510	50	130	118,138	0.3846	upside down cone
Phillips Petroleum Co.	23	1457	1520	63	115	116,485	0.5478	cylinder
Phillips Petroleum Co.	24	1431	1461	30	200	167,770	0.1500	cylinder
	1a	1737	1752	15	130	35,441	0.1154	cylinder
	1b	1755	1775	20	29	2,352	0.6897	upside down cone
Diamond Koch	1					37,793		
	2a	1690	1745	55	81	50,451	0.6790	stack pancakes
	2b	1776	1785	9	15	283	0.6000	upside down cone
Diamond Koch	2					50,734		
Diamond Koch	3	1723	1754	31	119	61,375	0.2605	stack pancakes
Diamond Koch	4	1700	1768	68	63	37,733	1.0794	upside down cone
Diamond Koch	5	1709	1734	25	82	23,502	0.3049	cylinder
	6a	1704	1737	33	82	31,022	0.4024	cylinder
	6b	1752	1768	16	36	2,899	0.4444	upside down cone
Diamond Koch	6					33,921		
Diamond Koch	7	1739	1774	35	101	49,917	0.3465	upside down cone
Diamond Koch	9	1756	1766	10	163	37,146	0.0613	cylinder
			Average	39	158	151793		

The average cavern in the Anadarko Basin has a height of 39ft and diameter of 158ft. The cavern is primarily cylindrical in shape with an average capacity of 151,793 barrels.

Table 2 Midland Basin Sonar Survey Summary

Company	Cavern No.	Main Roof	Bottom Depth (ft)	Ave. Height (ft)	Ave. Diameter	Cavern Volumn	Ht/W Ratio	Shape
	1a	2105	2165	60	60	30,199	1.0000	cylinder
	1b	2212	2315	103	160	368,647	0.6438	stack pancakes
	1c	2455	2530	75	220	507,505	0.3409	cylinder
	1d	2603	2650	47	382	958,867	0.1230	cylinder
Unocal/Union Oil Co.	1					1,865,217		
	2a	2055	2140	85	120	171,126	0.7083	upside down cone
	2b	2202	2290	88	255	800,012	0.3451	stack pancakes
	2c	2432	2488	56	230	414,169	0.2435	stack pancakes
	2d	2580	2660	80	181	366,421	0.4420	cylinder
Unocal/Union Oil Co.	2					1,751,728		
Mid-America Pipeline Co.	1	2540	2587	47	316	656,154	0.1487	cylinder
Mid-America Pipeline Co.	2	2550	2685	135	145	396,829	0.9310	stack pancakes
Mid-America Pipeline Co.	3	2640	2730	90	145	264,553	0.6207	upside down cone
Mid-America Pipeline Co.	4	2618	2713	95	130	224,463	0.7308	stack upside down cones
Mid-America Pipeline Co.	5	2623	2710	87	125	190,052	0.6960	stack upside down cones
Mid-America Pipeline Co.	6	2610	2665	55	200	307,579	0.2750	cylinder
Mid-America Pipeline Co.	7	2620	2682	62	134	155,645	0.4627	stack pancakes
Mid-America Pipeline Co.	8	2640	2715	75	160	268,432	0.4688	upside down cone
Mid-America Pipeline Co.	9	2607	2700	93	175	398,192	0.5314	stack upside down cones
	11a	2600	2627	27	44	7,308	0.6136	stack pancakes
	11b	2648	2730	82	70	56,175	1.1714	stack upside down cones
Mid-America Pipeline Co.	11					63,483		
	12a	2573	2621	48	85	48,486	0.5647	stack pancakes
	12b	2643	2710	67	107	107,245	0.6262	upside down cone
Mid-America Pipeline Co.	12					155,730		
Mid-America Pipeline Co.	13	2625	2738	113	87	119,578	1.2989	stack pancakes
Mid-America Pipeline Co.	14	2640	2746	106	94	130,947	1.1277	cylinder
Amoco Production Co.	1	2417	2682	265	75	208,402	3.5333	upside down cone w/long n
	2a	2335	2408	73	36	13,227	2.0278	stack upside down cones
	2b	2408	2425	17	273	177,136	0.0623	upside down cone
Amoco Production Co.	2					190,363		
	3a	2325	2382	57	23	4,216	2.4783	cylinder
	3b	2400	2525	125	76	100,942	1.6447	diamond
Amoco Production Co.	3					105,157		
	1a	1368	1450	82	55	34,679	1.4909	stack pancakes
	1b	1450	1507	57	146	169,869	0.3904	cylinder
Chevron Pipeline Co.	1					204,549		
	2a	1195	1354	159	15	5,002	10.6000	stack pancakes
	2b	1381	1512	131	78	111,428	1.6795	stack pancakes
Chevron Pipeline Co.	2					116,430		
	3a	1205	1435	230	24	18,522	9.5833	stack pancakes
	3b	1445	1483	38	115	70,261	0.3304	chevron
Chevron Pipeline Co.	3					88,783		
	1001a	977	1060	83	25	7,253	3.3200	upside down cone
	1001b	1080	1190	110	92	130,167	1.1957	stack pancakes
Alon USA, LP	1001					137,420		
	1004a	985	1085	100	23	7,396	4.3478	stack upside down cones
	1004b	1107	1200	93	59	45,261	1.5763	stack upside down cones
Alon USA, LP	1004					52,656		
	1005a	1070	1165	95	46	28,104	2.0652	stack upside down cones
	1005b	1205	1240	35	140	95,909	0.2500	upside down cone
Alon USA, LP	1005					124,013		
	1007a	995	1175	180	28	19,730	6.4286	stack pancakes
	1007b	1205	1245	40	128	91,625	0.3125	cylinder
Alon USA, LP	1007					111,355		
Oneok	1	2790	3020	230	200	1,286,238	1.1500	cylinder
Oneok	2	2728	2910	182	230	1,346,048	0.7913	bell
			Average	95	125	278717		

The average cavern in the Midland Basin has a height of 95ft and diameter of 125ft. The cavern shape varies from narrow cylindrical to stack pancakes to upside down cone shapes. The average capacity of the cavern is 278, 717 barrels.

Table 3 Michigan Basin Sonar Survey Summary

Company	Cavern No.	Main Roof	Bottom Depth (ft)	Ave. Height (ft)	Ave. Diameter	Cavern Volumn	Ht/W Ratio	Shape
Ohio Northwest Inc	LPG#2	3695	3905	210	100	293598	2.1000	cylinder
Ohio Northwest Inc	LPG#5	3755	3840	85	105	131018	0.8095	cylinder
Ohio Northwest Inc	Fee #6	3764	3942	178	116	334865	1.5345	cylinder
Phillips Petroleum C	1	1142	1230	88	128	201575	0.6875	upside down cone
Phillips Petroleum C	2	1135	1226	91	82	85547	1.1098	upside down cone
Consumers Power C	2-CC/7005	1990	2158	168	98	225577	1.7143	stack pancakes
Consumers Power C	3-CC/7006	1988	2186	198	120	398622	1.6500	stack upside down cones
Consumers Power C	1-C5/7007	1986	2142	156	192	804008	0.8125	stack upside down cones
Consumers Power C	2-C5/7008	2007	2146	139	204	808740	0.6814	cylinder
Consumers Power C	1-C4/7009	1986	2100	114	196	612281	0.5816	cylinder
Consumers Power C	2-C4/7010	1985	2134	149	182	690021	0.8187	stack upside down cones
Consumers Power C	1-C3/7011	1984	2134	150	180	679469	0.8333	cylinder
Consumers Power C	2-C3/7012	1982	2130	148	196	794891	0.7551	cylinder
Amoco Oil Co.	A-1	2345	2435	90	145	264553	0.6207	upside down cone
Amoco Oil Co.	A-3	2332	2426	94	148	287862	0.6351	cylinder
Amoco Oil Co.	A-5	2348	2448	100	155	335890	0.6452	upside down cone
Amoco Oil Co.	A-6	2345	2440	95	160	340014	0.5938	upside down cone
Amoco Oil Co.	A-8	2332	2430	98	140	268544	0.7000	upside down cone
Amoco Oil Co.	A-9	2348	2416	68	195	361503	0.3487	stack pancakes
Amoco Oil Co.	A-10	2346	2422	76	156	258581	0.4872	upside down cone
Sun Pipeine Co.	1	1188	1242	54	116	101588	0.4655	cylinder
Sun Pipeine Co.	2	1196	1264	68	98	91305	0.6939	stack pancakes
Sun Pipeine Co.	3	1180	1242	62	114	112651	0.5439	stack pancakes
Sun Pipeine Co.	4	1570	1668	98	98	131587	1.0000	stack pancakes
Sun Pipeine Co.	5	1602	1678	76	98	102047	0.7755	upside down cone
	6a	1170	1190	20	135	50960	0.1481	stack pancakes
	6b	1201	1248	47	160	168218	0.2938	upside down cone
Sun Pipeine Co.	6					219178		
Sun Pipeine Co.	7	1565	1645	80	110	135335	0.7273	stack pancakes
	9a	1498	1578	80	40	17895	2.0000	cylinder
	9b	1580	1656	76	70	52065	1.0857	stack pancakes
Sun Pipeine Co.	9					69960		
			Average	105.20	134.57	301935		

The average cavern in the Michigan Basin has a height of 105ft and diameter of 134ft. The cavern shape varies from narrow cylindrical to stack pancakes to upside down cone shapes. The average capacity of the cavern is 301,935 barrels.

Table 4 Appalachian Basin Sonar Survey Summary

Company	Cavern No.	Main Roof Depth (ft)	Bottom Depth (ft)	Ave. Height (ft)	Ave. Diameter (ft)	Calculated Cavern Volumn (bbls.)	Volume from reports (bbls)	Ht/W Ratio	Shape
NY LP Gas Storage	Harford#1	3025	3100	75	200	419,426	362,628	0.3750	bell
NY LP Gas Storage	Hartford#2	2927	2950	23	180	104,185	57430	0.1278	stack pancakes
NY LP Gas Storage	Hartford#3	3030	3198	168	100	234,878	236158	1.6800	diamond
Bath Petroleum Storage Inc	1	2976	3153	177	96	228,060	228381	1.8438	cylindrical
Bath Petroleum Storage Inc	2	2922	3078	156	126	346,258	157714	1.2381	
Bath Petroleum Storage Inc	3	2969	3084	115	108	187,534	186214	1.0648	
Bath Petroleum Storage Inc	4	2949	3030	81	100	113,245	146405	0.8100	cylindrical
Bath Petroleum Storage Inc	5	2929	3175	246	64	140,873	166286	3.8438	cylindrical
Bath Petroleum Storage Inc	6	2961	3165	204	63	113,200	201286	3.2381	cylindrical
Bath Petroleum Storage Inc	7	2950	3200	250	63	138,725	261452	3.9683	cylindrical
Bath Petroleum Storage Inc	9	3000	3515	515	34	83,234	86548	15.1471	
Bath Petroleum Storage Inc	10	3004	3512	508	20	28,409	28310	25.4000	
Bath Petroleum Storage Inc	11	3109	3492	383	7	2,624	2429	54.7143	
Bath Petroleum Storage Inc	12	3009	3524	515	8	4,608	4810	64.3750	
Bath Petroleum Storage Inc	13	2964	3474	510	32	73,014	73119	15.9375	
Ohio Fuel Gas Co			2352						
Standard Oil Co. Ohio		2001				80000			
Marathon-Ashland Ohio	GS-1	3630							
Marathon-Ashland Ohio	GS-2	3634							
Marathon-Ashland Ohio	GS-4								
Marathon-Ashland Ohio	GS-5								
Lake Undergd Storage Ohio	A--121	1996							
Lake Undergd Storage Ohio	A--122	1996				78568			
Lake Undergd Storage Ohio	124								
Lake Undergd Storage Ohio	B--303	1959	2410						
Lake Undergd Storage Ohio	B--304								
			Average	261.73	80.07	147,885	146,611		

Ohio data per Tom Tomastik personal communication and 1996, 1997, 2001 papers, no sonar data, not required in Ohio

The average cavern in the Appalachian Basin has a height of 261ft and diameter of 80ft. The cavern shape is mostly cylindrical. The average calculated capacity of the cavern is 147,885 barrels. The actual cavern capacity is 146,611 barrels, which is less than 1% difference from the calculated cavern capacity.

4. GEOMECHANICAL ANALYSIS OF SALT CAVERNS

There are four basic geomechanical processes that limit maximum and minimum pressures in a bedded salt cavern. These are:

- The tensile fracturing pressure for the salt material and interbedded non-salt materials,
- The formation stresses induced by cavern pressure decline or increase, at which bedding plane slip might occur between heterogeneous material layers,

- The minimum cavern pressure that might induce roof instability or excessive closures.
- The creep response of the material, which again is a function of the cavern pressure. Low cavern pressures increase the creep response in the surrounding salt material thereby accelerating the closure process

Terralog is continuing our investigation and performing various simulations to determine the minimum and maximum pressure limits for thin bedded salt caverns in a variety of typical settings occurring within the Permian Basin Complex and the Michigan and Appalachian Basins.

4.1 Cavern Model Configurations and Loading Conditions

Terralog has developed a set of three dimensional geomechanical models to investigate cavern deformation and bedding plane slip for a variety of cavern configurations. Table 5 summarizes the geomechanical models developed for this project. Numerical simulations include a baseline case and various scenarios for different height to diameter cavern ratio, different salt roof beam thickness, a range of cavern depth, single and multiple caverns and varying interface properties. Each cavern simulation involves one year of pressure cycling with minimum, mean, and maximum cavern pressure gradient of 0.35 psi/ft, 0.50 psi/ft, and 0.85 psi/ft, respectively. Figure 4 shows the typical single cavern pressure cycle at the depth of 2500 ft.

Table 5 Cavern Configuration Simulation Matrix

		Cavern Depth		Cavern Dimension				Salt Roof Beam	Interface Properties	Comments
Simulation Model #	Cavern Shape	Main Roof Depth (ft)	Salt Temperature (K) *	H/D Ratio	Height (ft)	Diameter (ft)	Cavern Volume (ft^3)	Thickness (ft)	Friction Angle (deg)	Evaluation
Typ1A	Rectangular Cylinder	2500 (762 m)	304 (31 C)	1/2	100 (30.5m)	200 (61m)	3.14e6 (5.60e5 bbls)	40 (12m)	15	Base Line Model
Typ1B	Rectangular Cylinder	2500 (762 m)	304 (31 C)	1/4	100 (30.5m)	400 (122m)	1.26e7 (2.23e6 bbls)	40 (12m)	15	Ratio of Cavern Height/Diameter
Typ1C	Rectangular Cylinder	2500 (762 m)	304 (31 C)	1/6	100 (30.5m)	600 (183m)	2.83e7 (5.03e6 bbls)	40 (12m)	15	Ratio of Cavern Height/Diameter
Typ1D	Rectangular Cylinder	2500 (762 m)	304 (31 C)	1/8	100 (30.5m)	800 (244m)	5.03e7 (8.95e6 bbls)	40 (12m)	15	Ratio of Cavern Height/Diameter
Typ1E	Rectangular Cylinder	2500 (762 m)	304 (31 C)	1	100 (30.5m)	100 (30.5m)	7.85e5 (1.40e5 bbls)	40 (12m)	15	Ratio of Cavern Height/Diameter
Typ2A	Rectangular Cylinder	2500 (762 m)	304 (31 C)	1/2	100 (30.5m)	200 (61m)	3.14e6 (5.60e5 bbls)	0	15	Thicknes of Salt Roof Beam
Typ2B	Rectangular Cylinder	2500 (762 m)	304 (31 C)	1/2	100 (30.5m)	200 (61m)	3.14e6 (5.60e5 bbls)	80 (24.4m)	15	Thicknes of Salt Roof Beam
Typ3A	Rectangular Cylinder	2500 (762 m)	304 (31 C)	1/2	100 (30.5m)	200 (61m)	3.14e6 (5.60e5 bbls)	40 (12m)	5	Interface Slippage
Typ3B	Rectangular Cylinder	2500 (762 m)	304 (31 C)	1/2	100 (30.5m)	200 (61m)	3.14e6 (5.60e5 bbls)	40 (12m)	30	Interface Slippage
Typ4A	Rectangular Cylinder	2500 (762 m)	304 (31 C)	1/2	100 (30.5m)	200 (61m)	3.14e6 (5.60e5 bbls)	40 (12m)	15	Hydrostatic Cavern Pressure for 15 years
Typ5A	Rectangular Cylinder	1500 (457 m)	296 (22 C)	1/2	100 (30.5m)	200 (61m)	3.14e6 (5.60e5 bbls)	40 (12m)	15	Cavern Depth
Typ5B	Rectangular Cylinder	3500 (1067 m)	312 (39 C)	1/2	100 (30.5m)	200 (61m)	3.14e6 (5.60e5 bbls)	40 (12m)	15	Cavern Depth
Typ6A	Two Vertical Rectangular Cylinders	2500 (762 m)	304 (31 C)	1/2	100 (30.5m)	200 (61m)	6.28e6 (1.12e6 bbls)	40 (12m)	15	Multiple Vertical Caverns
Typ6B	Three Vertical Rectangular Cylinders	2500 (762 m)	304 (31 C)	1/2	100 (30.5m)	200 (61m)	9.42e6 (1.68e6 bbls)	40 (12m)	15	Multiple Vertical Caverns
Typ7A	Two Horizontal Rectangular Cylinders	2500 (762 m)	304 (31 C)	1/2	100 (30.5m)	200 (61m)	6.28e6 (1.12e6 bbls)	40 (12m)	15	Multiple Horizontal Caverns
Typ7B	Three Horizontal Rectangular Cylinders	2500 (762 m)	304 (31 C)	1/2	100 (30.5m)	200 (61m)	9.42e6 (1.68e6 bbls)	40 (12m)	15	Multiple Horizontal Caverns

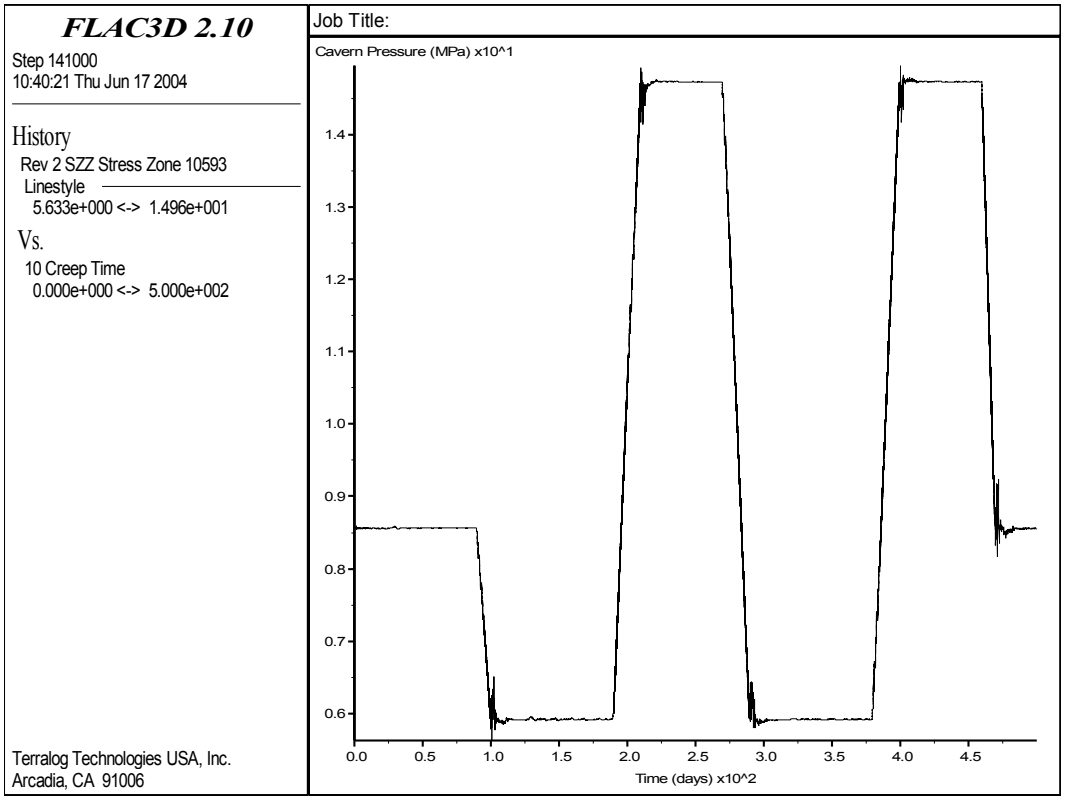

Figure 4: Cavern Pressure Single Year Cycle

Three dimensional geomechanical numerical simulations of thin-bedded salt caverns are applied to model typical real caverns as surveyed in the Permian, Michigan and Appalachian Basins. Multiple cavern configurations are developed using Flac3D to investigate the bedding plane slips and cavern deformation. The baseline model configuration is a cylindrical shaped cavern 100 ft in height and 200 ft in diameter. The cavern lies at the depth of about 2500 ft below the surface. Figure 5 shows the three dimensional single cavern baseline configuration modeled after a typical thin-bedded salt cavern. Figure 6 shows another typical multiple cavern configuration with shale interbed being modeled in Flac3D.

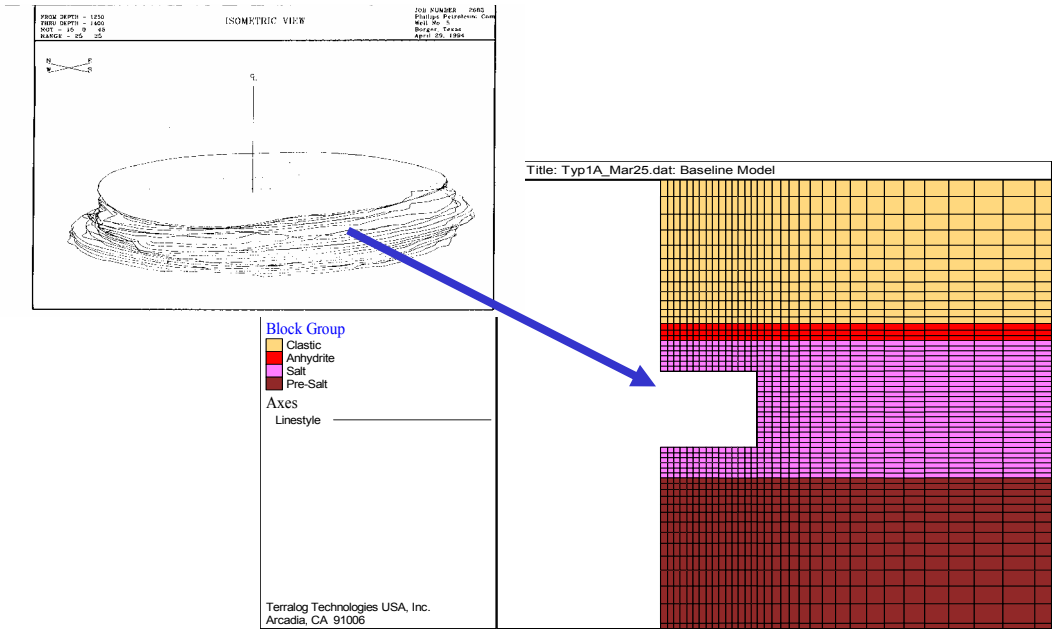

Figure 5: Three dimensional single cavern baseline model.

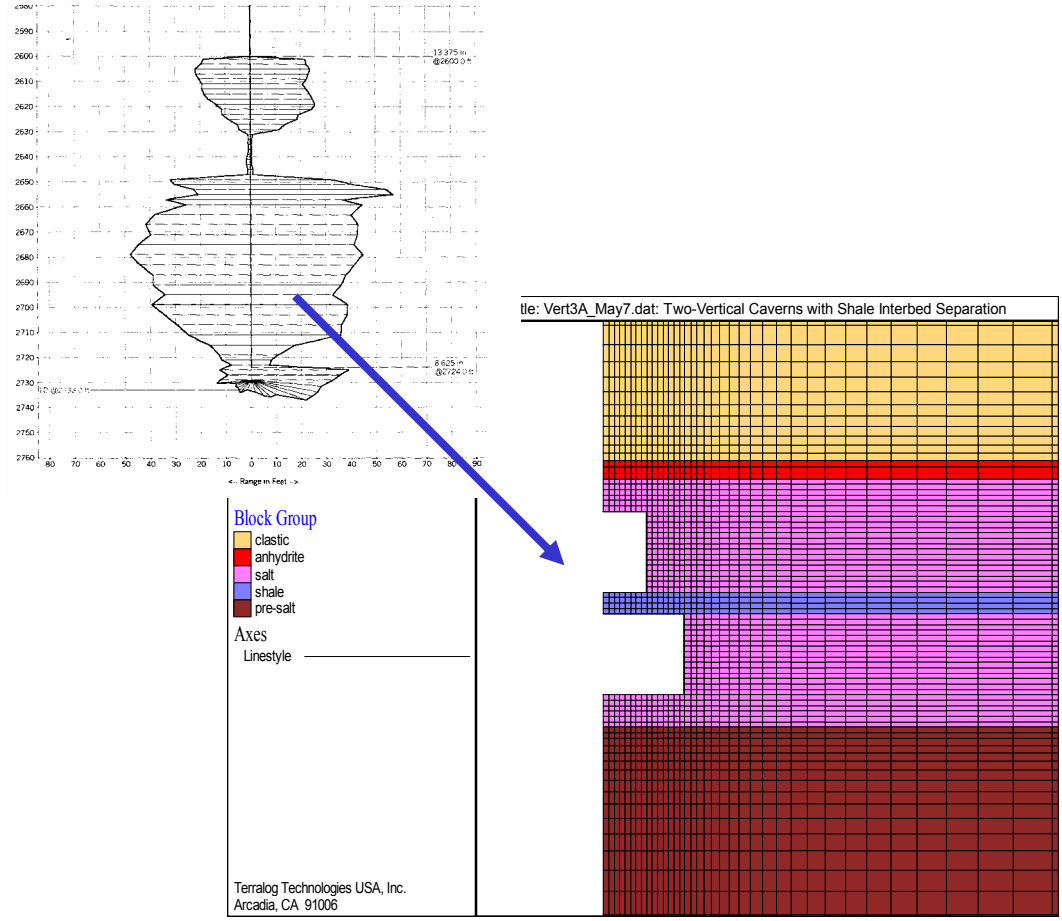

Figure 6: Three dimensional multiple vertical caverns model.

4.2 Salt Material Modeling

An empirical creep law based on the Waste Isolation Pilot Plant (WIPP) Program has been implemented by Itasca, Inc. for Flac3D creep material modeling. To account for the plastic and other failure mechanisms in standard bedded salt behaviors, the WIPP creep model are combined with the Drucker-Prager plasticity criterion, WIPP-Creep Viscoplastic Model in FLAC 3D. In order to simulate available material, the viscoplastic model in FLAC was modified by Terralog. The three principal modifications are:

1. Damage accumulation during primary loading;
2. Material failure and volumetric dilation after the Drucker-Prager failure criterion has been reached;
3. Loading-unloading response using initial stiffness properties, i.e. properties of undamaged material.

Damage accumulation during primary loading was achieved by introducing a deformation dependent shear modulus *G*. The magnitude of *G* has a nonlinear dependence on the second deviatoric stress invariant. A change in the shear modulus induces a change in the volumetric response as well. Once the state of stress satisfies the Drucker-Prager criterion, the material starts to dilate and its strength reduces gradually to zero.

Experimental data of the Permian salt show that during unloading and subsequent reloading, the material response is determined by initial undamaged stiffness properties. This characteristic was implemented as well and is essential to study cyclic loading. Figure 7 below shows the creep response of Permian salt at 100°C and is compared with experimental data from Figure C.17, reference [Pfeifle et al., 1983]. Numerical creep data for different temperature is easily obtained by changing the temperature in the input file, which is being used to calculate the secondary creep rate.

For each simulation a vertical stress is developed consistent with the density of overlying sediments (i.e. increasing with depth and equivalent to $\sigma_v \approx \int \rho g \, dz$). Lateral displacements at the outer radius of the model are fixed, so that horizontal stresses develop consistent with the vertical load and the Poisson Ratio for the various lithology layers. The general simulation process may be summarized as follows:

1. Define initial geologic layers and initial stress conditions;
2. Excavate cavern, apply an internal cavern pressure equal to the hydrostatic head of water (about 15MPa at a depth of 1500m);
3. Allow model to run and stresses to creep and equilibrate for 3 months;
4. Impose a 1-year pressure cycle in which cavern pressure increases to 30MPa in 3 months, returns to 15MPa after 6 months, decreases to 0MPa after 9 months, and returns to 15MPa. This is followed by about 30 days of steady state creep and equilibrium.

For each parametric simulation we evaluate roof displacements, cavern sidewall displacements, and bedding plane slip at various lithology interfaces.

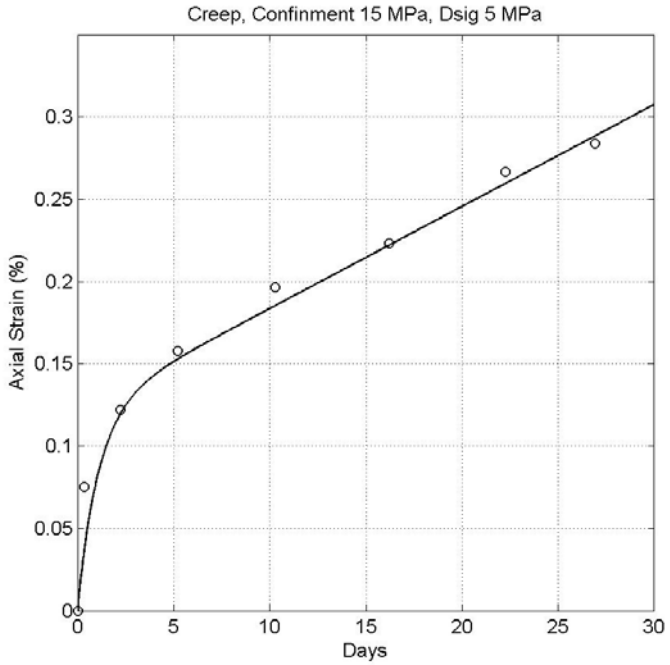

Figure 7: Creep response of Permian Salt. 15 MPa confinement pressure, 5MPa stress difference. The temperature of the simulation equal to 100°C

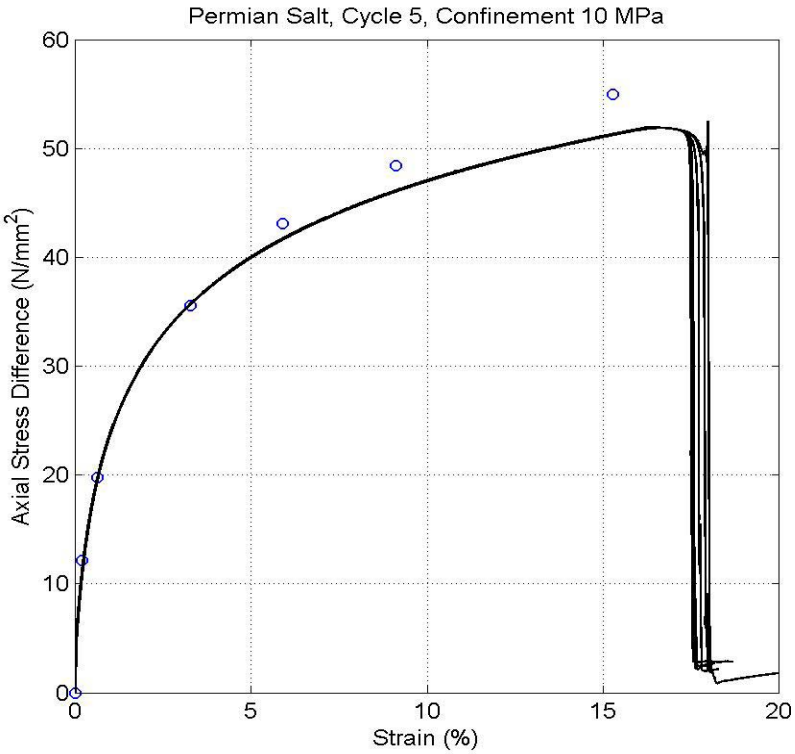

Figure 1: Principal stress difference (MPa) versus axial strain (%) of Permian salt subjected to 10 MPa confinement pressure, shown for 6 different discretizations of a unit cube.

4.3.1 Multiple Horizontal Cavern Simulations

Numerical models for a variety of multiple horizontal caverns configurations have been developed and applied to investigate cavern integrity and interaction between nearby caverns.

Table 6 summarizes the main parameters of this investigation. The geometric layout of each cavern is given by an H/D ratio of (1/2), i.e. a total height of 30 m (98.4 ft) and a diameter of 60 m (196.8 ft). These dimensions correspond to a cavern volume of 84,780 cubic meters (2,991,679 ft^3). Each cavern simulation involves one year of pressure cycling at a constant temperature of 31 degrees Celsius (304 degrees Kelvin) and with minimum, mean, and maximum cavern pressures equal to the single cavern studied earlier. The baseline case is given by two identical horizontal caverns located at a center-to-center distance of 120 m (393.6 ft), equal to 2 cavern diameters. Figure 9 shows the configuration of the three dimensional multiple horizontal cavern baseline model.

Table 6: Simulation matrix for multiple horizontal caverns numerical investigations.

Simulation Number	Number of Caverns	Cavern Height	Cavern Diameter	Center Distance	Pressure
1	2	30 m (98.4 ft)	60 m (196.8 ft)	120 m (393.6 ft)	Hydrostatic
2	2	30 m (98.4 ft)	60 m (196.8 ft)	120 m (393.6 ft)	Cyclic
3	2	30 m (98.4 ft)	60 m (196.8 ft)	180 m (590.4 ft)	Hydrostatic
4	2	30 m (98.4 ft)	60 m (196.8 ft)	180 m (590.4 ft)	Cyclic

In this subsection we summarize the numerical results of the baseline model comprised of two identical caverns with a center to center distance of 120 m (393.6 ft) (equal to two cavern diameters) and 1-year cyclic pressure operations. Similar to the one cavern investigation considered in the previous section, we first determine the state of stress in the salt and overburden in equilibrium with a hydrostatic cavern pressure of 8.8 MPa (1276 psi).

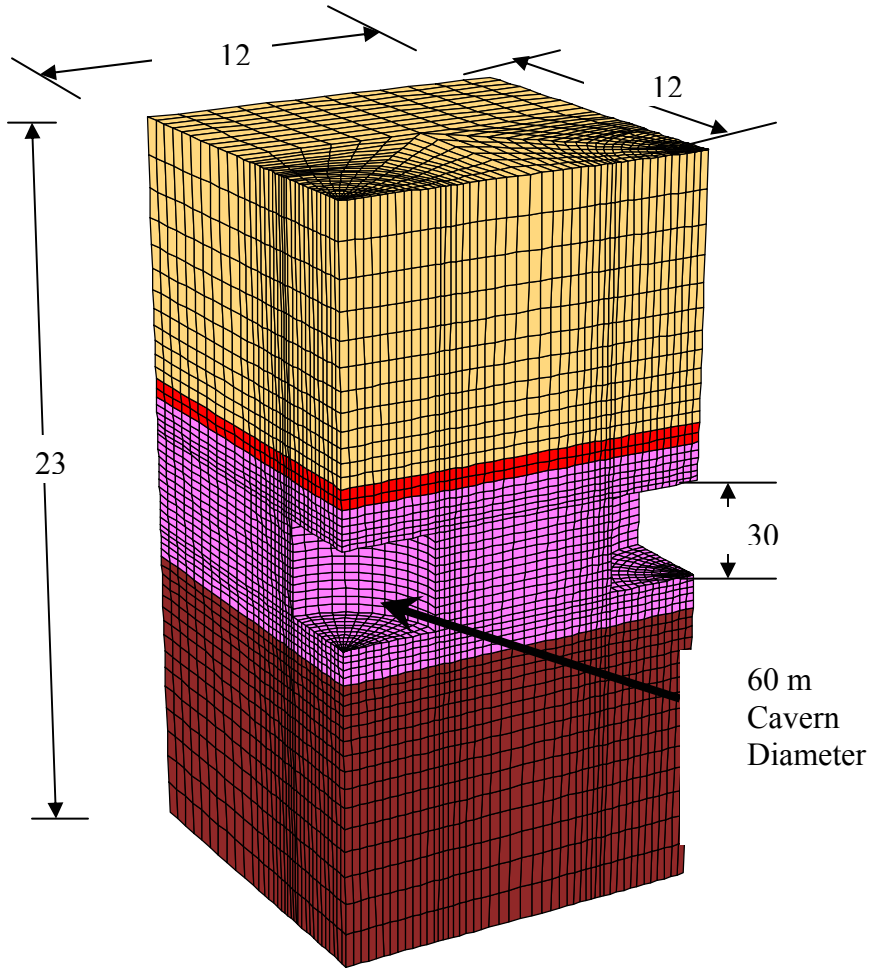

Figure 9: Three dimensional multiple horizontal caverns baseline model.

Multiple Horizontal Cavern Baseline Simulation Results

We select the displacement magnitude as a kinematics quantity to describe and visualize cavern interaction. Figure 10 shows the displacement magnitude at equilibrium with a hydrostatic cavern pressure of 8.8 MPa (1276 psi). Even though the magnitude of the displacement is non-zero in the intermediate region of the two caverns, the magnitude of the induced stress is small and stays in the elastic range, i.e. the stresses do no generate any damage in this region, as shown in Figure 11. This figure also shows that micro-cracks are generated only in proximity of the caverns and the extend of slippage between the cavern roof and the anhydrite layer.

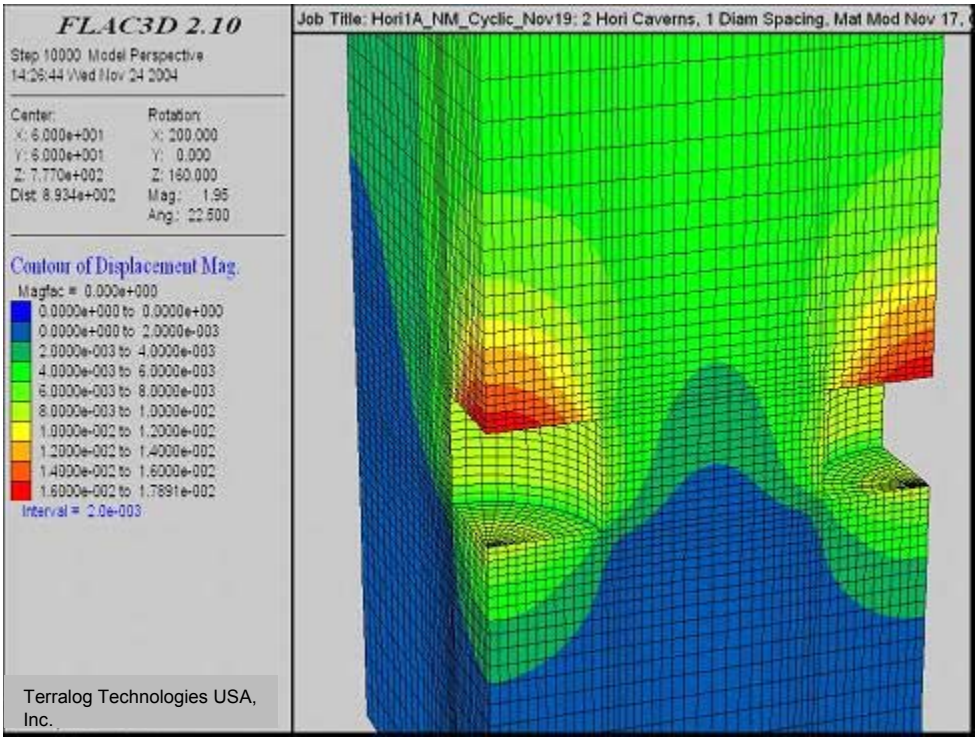

Figure 10: Plot of displacement magnitude for caverns in equilibrium with cavern pressure of 8.8 MPa (1276 psi). Center to center distance is 2 cavern diameters.

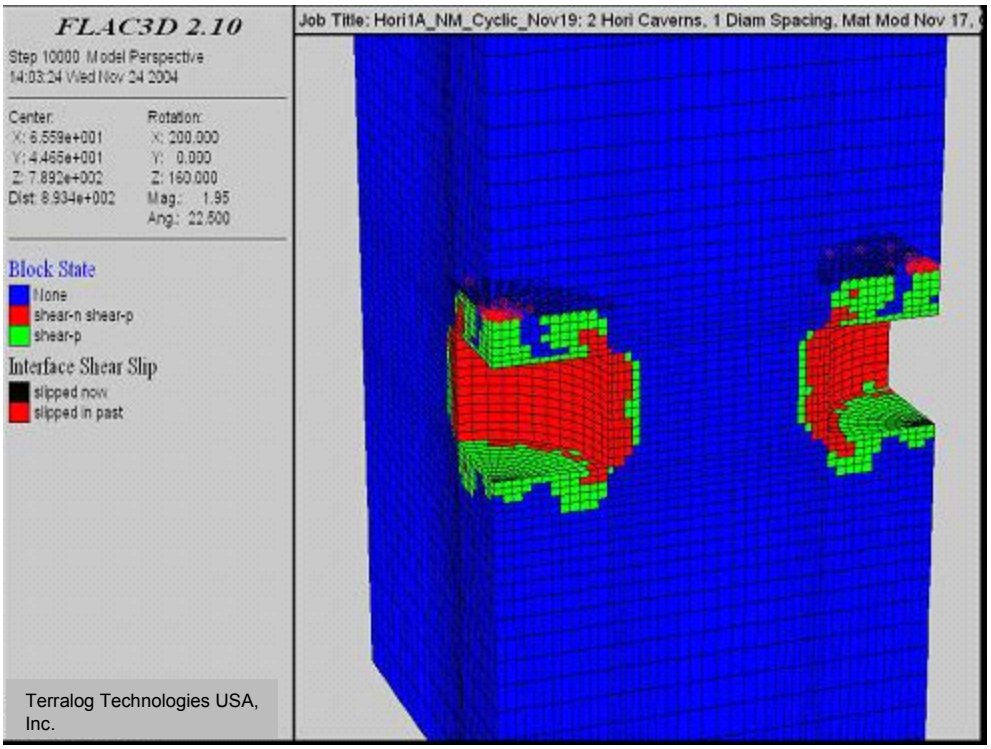

Figure 11: Distribution of damage and interface slip of caverns with center to center distance of 2 cavern diameters. Cavern pressure is 8.8 MPA (1276 psi).

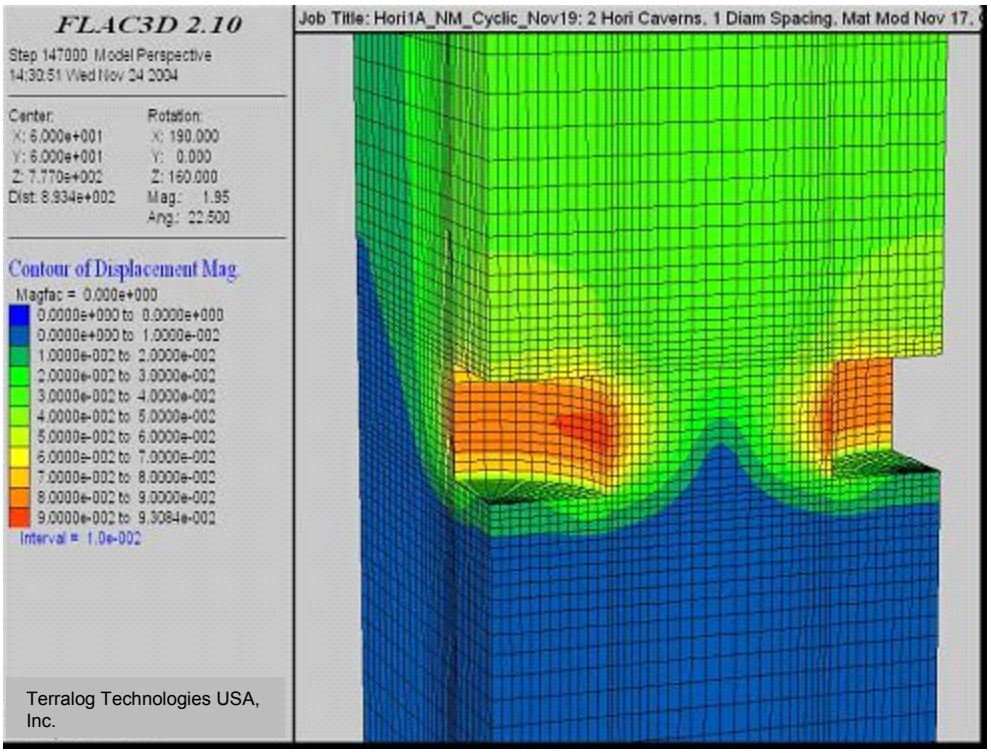

Figure 12: Contour plot of displacement magnitude after 1 year of pressure cycling. Center to center distance is 2 cavern diameters.

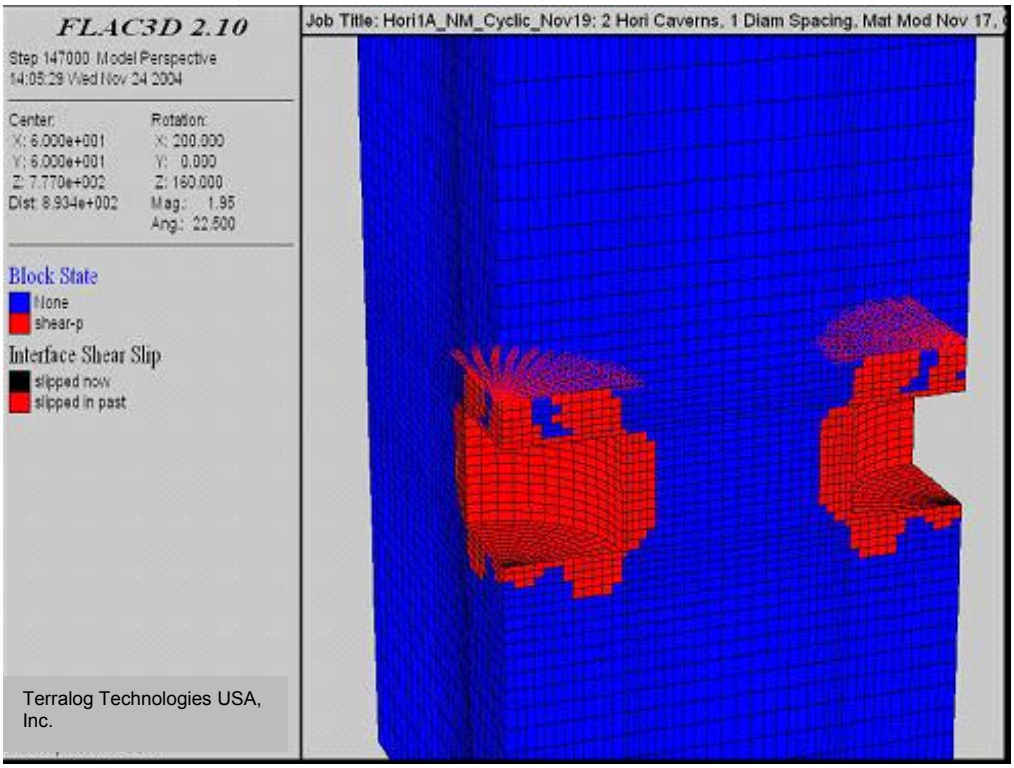

Figure 13: Distribution of micro-cracks and location of interface slip after 1 year of pressure cycling. Center to center distance is 2 cavern diameters.

Figure 12 and Figure 13 show the results of the baseline case after 1 year of pressure cycling. From Figure 10 and Figure 11, an increase in the lateral displacement of the cavern side wall from approximately 0.01 m (0.0328 ft) to 0.09 m (0.2952 ft) can be noted. An increase in the vertical displacement of the cavern roof also occurs. However, no additional cracks are generated. This may be observed by comparing Figure 11 and Figure 13. This can be explained by the viscous response of salt. Creep tends to reduce the magnitude of any deviatoric stress component in the salt, which ultimately approaches a pure hydrostatic state of stress. Therefore, the cavern closure in this particular case is due to creep deformation only and not to additional damage in the material.

The amount of damage is larger compared to the results of the one cavern baseline case. The model for the baseline case involving one cavern assumes axisymmetric geometry and loading. Multiple cavern simulation results indicate that the interaction of these two caverns, located at a center to center distance of two cavern diameters, does affect the response during pressure cycling. The interaction is best seen by the increase in the lateral wall displacement, although no additional damage is generated.

Influence of Horizontal Caverns Separation Distance on Cavern Deformation and Stability

In this subsection, we investigate the effect of horizontal cavern distance on the displacement magnitude and on the accumulation of damage. We increase the center-to-center distance of two identical caverns to 180 m (590.4 ft), which is equivalent to three cavern diameters. Figure 14, which is the equilibrium configuration with cavern pressure of 8.8 MPa (1276 psi), shows that the magnitude of the displacement vanishes in the part of the region between the two caverns, compare with Figure 15. However, it is interesting to observe that at equilibrium the vertical roof displacement and the lateral movement of the side wall coincide with that found in our baseline case.

The displacement magnitude increases after a one-year pressure cycling, as shown in Figure 15. This applies for the cavern roof as well as for the side wall. However, it should be pointed out that the lateral movement of the vertical wall is somewhat smaller when compared to the baseline model (Figure 14).

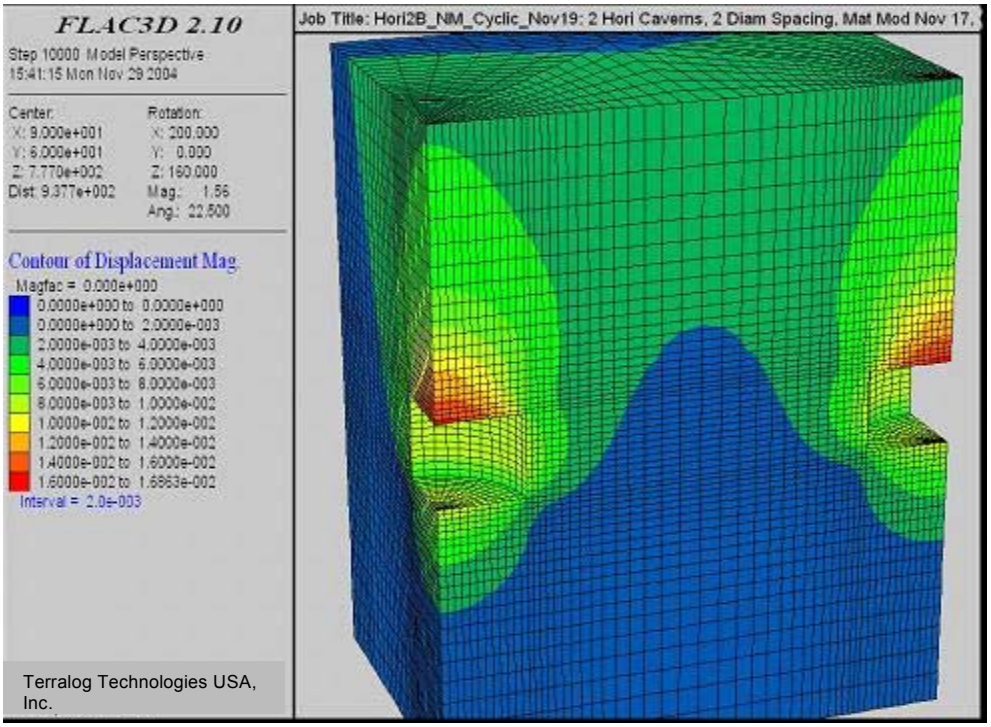

Figure 14: Plot of displacement magnitude for caverns in equilibrium with cavern pressure of 8.8 MPa (1276 psi). Center to center distance is 3 cavern diameters.

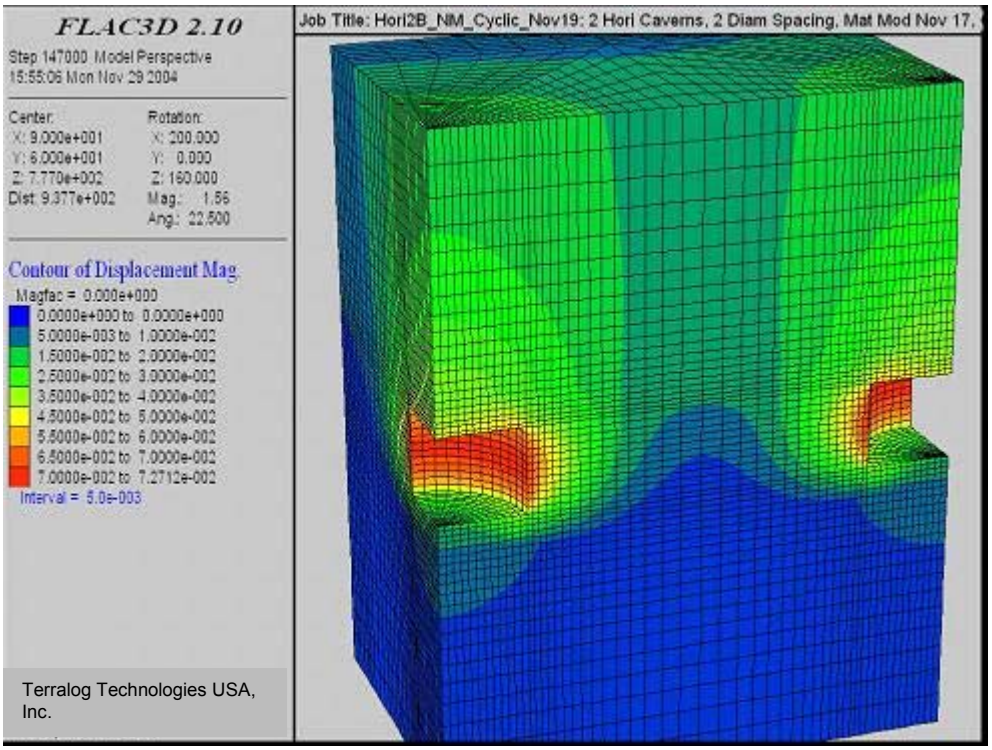

Figure 15: Plot of displacement magnitude for caverns after one year of pressure cycling. Center to center distance is 3 cavern diameters.

5. SUMMARY AND CONCLUSIONS

Designing bedded salt caverns for natural gas and liquid storage should take into account the mechanical properties of natural bedded salt in order to perform accurate numerical simulations. In this research, a modified creep viscoplastic model has been developed and implemented in Flac3D to simulate the response of cavern embedded into layered salt of the Permian, Michigan and Appalachian Basins. The original viscoplastic model is based on an empirical creep law developed for Waste Isolation Pilot Plant (WIPP) Program and combined with the Drucker-Prager yield model to describe damage. Experimental data for the Permian salt provided by Pfeifle et al. 1983, are used to validate the basic assumptions made in the development of the damage model. A number of one element numerical simulations have been performed to calibrate the model, such as uniaxial tension test, uniaxial compression test, triaxial compression test and creep test. The numerical results show that the modified creep model approximates experimental data reasonable well.

With the modified creep viscoplastic model, bedded salt caverns for natural gas storage are simulated numerically considering various layer properties, e.g. salt, anhydrite layer, overburden clastic, and underlying pre-salt. A baseline model using a predefined cyclic pressure history is used to determine the stress distribution around the cavern and the distribution of damage with possible implication on the salt roof stability. Different design parameters are varied to determine the influence on the accumulation of damage in salt and on the deformation of the salt cavern. These are the lower limit of the cavern pressure, the cavern pressure history, operational conditions, and cavern size expressed in terms of height/diameter ratio, overburden stiffness, interface properties and roof thickness.

The baseline model of a single cavern suggests that at equilibrium with the hydrostatic cavern pressure, a shear stress distribution around the cavern top and bottom corners. Furthermore, in order to reach equilibrium micro-cracks have been induced around the cavern sidewalls and slippage along the interface between the salt and anhydrite layers occurs. During cyclic pressure operations, no additional micro-cracks are generated. However additional interface slip occurs mainly due to the minimum cavern pressure reached during operations. Additional cavern closure during cycling is primarily due to creep deformation and interface slippage.

The amount of damage and interface slippages in the cavern with an H/D ratio of (1/4) after one year of pressure cycling increase and also extend over larger regions. For the smaller cavern with an H/D ratio of (1/1), the damaged region is smaller and involves primarily the vertical wall. Interface slippage occurs only in the interface above the cavern.

The effect of the overburden stiffness on the cavern response shows that by reducing the stiffness by an order of magnitude, for example, a substantial part of the overburden weight is supported by the anhydrite layer and the cavern roof itself. As a consequence the interface and the anhydrite layer fail and the vertical displacement of the cavern roof increases with a corresponding increase in damage and slippage. Doubling the salt roof thickness does reduce the extension of damage in the roof itself. The transfer of horizontal stress between the salt and the

anhydrite layer is still in excess of the interface strength, therefore slip conditions are present. Doubling the roof thickness, does not, as expected, influence the response along the vertical cavern wall.

Numerical models are also developed to analyze and to determine the interaction of multiple caverns. In particular, the influence of the center to center distance of multiple caverns on displacement magnitude and accumulation of damage, are investigated. We also consider the mechanical properties and the elasto-plastic response of non-salt strata above and below the salt cavern. Various formations are simulated in FLAC3D, including an elasto-plastic anhydrite layer, a Mohr-Coulomb type overburden clastic and an elastic underlying presalt.

The interaction of multiple horizontal bedded salt caverns is evaluated to determine the minimum save distance without compromising safety issues. Similar to the single cavern analyses, a baseline case is considered, which is first subjected to a hydrostatic pressure loading of 8.8 MPa (1276 psi) and then to pressure cycling over a one year period.

The geometric dimensions of each cavern are equal to the baseline case of the single cavern model. However, the important value is the center to center distance, which initially is selected as 120 m (393.6 ft) and corresponds to 2 cavern diameters. Subsequently, to quantify the cavern to cavern interaction, this distance is increased to 180 m (590.4 ft), which corresponds to 3 cavern diameters, see Table 6.

To describe und visualize the mutual cavern interaction, we select the displacement magnitude as our basic variable. Comparing the corresponding values for the same loading conditions, but different cavern distances, we find that for a distance of 180 m (590.4 ft) all interactions vanish. This is in contrast to the results obtained for the 120 m (393.6 ft) center to center distance, where an increase in the lateral wall displacement is noted during pressure cycling. In the latter case, even though the interaction extends throughout the interconnecting region, the generated stresses are small and remain elastic, i.e. no permanent damage.

In summary, cavern development and operation in thin bedded salt provides additional challenges over conventional domal salt cavern operations. The challenges are related to the heterogeneous material properties, the resulting differences in fracture pressure, and the potential for bedding plane slip across the cavern height (leading to gas migration risk) and within the roof and caprock (leading to roof caving and well shear damage risk). Notwithstanding these challenges, however, appropriate geologic characterization and geomechanical assessment efforts can be applied to safely develop and operate caverns in bedded salt formations.

6. REFERENCES

American Gas Association (AGA), 1998 Survey of Underground Storage of Natural Gas in the United States and Canada.

API, 1994, "Design of Solution-Mined Underground Storage Practices," API Recommended Practice 1114, American Petroleum Institute, Washington, DC, June.

Bruno, M.S., Dewolf, G., and Foh, S. (2000): Geomechanical analysis and decision analysis for delta pressure operations in gas storage reservoirs, Proc. AGA Operations Conf., Denver, CO, May 7-9.

Cromwell, D.W., 1984, The Upper Delaware Mountain Group, Permian (Guadalupian), southeast New Mexico and West Texas in Mazzullo, S.J., ed., The Geologic Evolution of the Permian Basin section, Midland, Texas, Permian Basin Section – SEPM, Symposium, p.32-34

DeVries K.L., Mellegard K.D., Callahan G.D., 2002, Salt Damage Criterion Proof-of-Concept Research, Technical Report RSI-1675, November 2002.

Fossum A.F. and Fredrich J.T., 2002, Salt mechanics primer for near-salt and sub-salt deepwater Gulf of Mexico field developments. SANDIA Report, SANDIA 2002-2063, July 2002.

Gustavson, T.C., Finley, R.J. and McGillis, K.A., 1980, Regional Dissolution of Permian Salt in the Anadarko, Dalhart and Palo Duro Basins of the Texas Panhandle, Texas Bureau of Economic Geology, Report of Investigations No. 106

Hoffman E.L. and Ehgartner B.L., 1992, Evaluating the Effects of the Number of Caverns on the Performance of Underground Oil Storage Facilities. Sandia Report, SANDIA-92-2183C, 1992

Hovorka, S.D. and Nava R., 2000, Characterization of Bedded Salt for Storage Salt Caverns – A Case Study from the Midland Basin, Texas, National Petroleum Technology Office, DOE/BC/15030-1

IOGCC, 1995, "Natural Gas Storage in Salt Caverns - A Guide for State Regulators," Interstate Oil and Gas Compact Commission, Oklahoma City, OK, October.

IOGCC, 1998, Natural Gas Storage in Salt Caverns, A Guide for State Regulators, Interstate Oil and Gas Compact Commission, 45pp.

Jizba, D. and Nur, A, 1990, Static and dynamic moduli of tight gas sandstones and their relation to formation properties, SPWLA 31st Annual Logging Symposium, Paper BB

Johnson, K.S. and Gonzales, S., 1978. Salt Deposits in the United States and RegionalGeological Characteristics Important for Storage of Radioactive Wastes. Office of Waste Isolation, Union Carbide Corp., US Dept of Energy, Y/OW1/SUB-7414/1, 188 pp.

Johnson, K.S. and Gonzales, S., 1978, Salt Deposits in the United States and Regional Geologic Characteristics Important for Storage of Radioactive Waste, Office of Waste Isolation, Y/OWI/SUB-7414/1

Johnson, K.S., 1986, Salt Dissolution and Collapse at the Wink Sink in West Texas, Office of Nuclear Waste Isolation, Battelle Memorial Institute, BMI/ONWI-598

Lytle, W.S., 1963, Underground Gas Storage in Pennsylvanian, Pennsylvanian Geological Survey, Bulletin M46.

McGillis, K.A. and Presley, M.W., 1981, Tansill, Salado, and Alibates Formations: Upper Permian Evaporite/ Carbonate Strata of the Texas Panhandle, Texas Bureau of Economic Geology, Geological Circular 81-8

McGookey, D., Gustavson, T.C. and Hoadley, A.D., 1988, Regional Structural Cross Sections, Mid Permian to Quaternary Strata, Texas Panhandle and Eastern New Mexico, Distribution of Evaporites and Areas of Evaporite Dissolution and Collapse, Texas Bureau of Economic Geology

McGookey, D., Gustavson, T.C. and Hoadley, A.D., 1988, Regional Structural Cross Sections, Mid Permian to Quaternary Strata, Texas Panhandle and Eastern New Mexico, Distribution of Evaporites and Areas of Evaporite Dissolution and Collapse, Texas Bureau of Economic Geology

Michigan State University, www.geo.msu.edu/geo333/miBasin.html

Munson, D.E., 1998, Analysis of Multistage and other Creep Data for Domal Salts, Sandia Report, SAND98-2276, 1998.

Munson, D.E.,1999, Multimechanism-Deformation Parameters of Domal Salts using Transient Creep Analysis, Sandia Report, SAND99-2104, 1999.

Neal, J.T. and Magorian, T.R., 1995. Geological Site Characterization Requirements for Storage and Mining is Salt. Proceedings Solution Mining Research Institute Spring Meeting, New Orleans LA, 19 pages.

Nieland J.D. and Mellegard K.D., 2002, Storage of Chilled Natural Gas in Bedded Salt Storage Caverns Economic and technical Feasibility. SMRI Spring Meeting, Alberta Canada, 2002.

Ohio Department of Natural Resources, 2002, Report on Ohio Mineral Industries, complied by Mark E. Wolfe.

Pfeifle, T.W., Mellegard, K.D., Senseny P.E., 1983, Preliminary constitutive properties for salt and nonsalt rocks from four potential repository sites. Technical Report. RE/SPEC Inc., July 1983.

Pfeifle, T.W., Vogt, T.J., Brekken G.A.,1995, Correlation of Chemical, Mineralogic and Physical Characteristics of Gulf Coast Dome Salt to Deformation and Strength Properties. SMRI 1996 Spring Meeting, Houston, TX, 1995.

Senseny P.E., Triaxial Compression Creep Tests on Salt from the Waste Isolation Pilot Plant, Topical report RSI-0294, 1986.

Smosna, R. and Patchen, D., 1978, Silurian Evolution of Central Appalachian Basin, American Association of Petroleum Geologists, Bulletin, v.62, no.11, p.2308-2328.

Stone and Webster Engineering Corp., 1983, Major Salt Beds of the Palo Duro and Dalhart Basins, Texas, Office of Nuclear Waste Isolation, Battelle Memorial Institute, BMI/ONWI-518

Tomastik, T.E., 1996, An Examination of the Geology of the Bass Islands and Salina groups in Ohio and Its Effect on Salt Solution Mining and Underground Storage, Solution Mining Research Institute, Meeting Paper, Oct.20-23, 1996, p.175-206.

Tomastik, T.E., 1997, The Sedimentology of the Bass Islands and Salina Groups in Ohio and Its Effect on Salt Solution Mining and Underground Storage, USA, in Carbonates and Evaporites, Friedman, Gerald M. Editor, vol.12, no.2, p.236-253.